Microfluidic circuits with tunable flow resistances

Eric W. Lam and Gregory A. Cooksey
Department of Bioengineering, University of Washington, Seattle, Washington 98195

Bruce A. Finlayson
Department of Chemical Engineering, University of Washington, Seattle, Washington 98195

Albert Folch[a)]
Department of Bioengineering, University of Washington, Seattle, Washington 98195

(Received 1 May 2006; accepted 5 September 2006; published online 18 October 2006)

Microfluidic devices, due to their conveniently small size and the unique physicochemical behavior of fluids in microscale volumes, have become essential tools in many areas of science and technology. Fluid flow in microchannels, microvalves, and micropumps have many parallels with electrical current through wires, switches, and current sources of microelectronic circuits. The equivalent of a variable resistor, however, is still unavailable. Here the authors present addressable microarrays of deformable elements producing sixteen levels of flow resistance. Using a purely resistive electrical circuit analog, they predict the steady-state output of a three-inlet mixer. © *2006 American Institute of Physics*. [DOI: 10.1063/1.2363931]

The fabrication of microfluidic devices in the elastomer poly(dymethysiloxane)[1] (PDMS) has enabled the integration of active components that, when deformed, act as microvalves (on/off[2–4] or leaky[5]), peristaltic micropumps,[3,6] and micromixers.[7] Fluid flow can be powered by capillarity, hydrostatic pressure, injection pumps, electro-osmosis, or micropumps.[8] While PDMS microvalves allow for step changes in flow resistance, gradual control of constant flow rates invariably requires physical manipulation of the sources that drive the fluids. In many settings, such manipulation is not practical (e.g., inside a tissue culture incubator) and/or cannot be scaled up to a large number of inputs (e.g., in a portable device).

Here we demonstrate microfluidic "resistors" (μFRs), microchannel segments whose height can be constricted to increase flow resistance. As shown in Fig. 1, the devices consist of a stack of three bonded PDMS layers made, as previously reported,[7] by standard soft lithography. The middle layer is a ~11-μm-thick PDMS membrane that is sandwiched between two microstructured PDMS layers. The top layer contains the fluid-carrying microchannels (~50 μm high, ~400 μm wide) and the bottom layer contains orthogonally oriented microchannels ("pneumatic lines," ~50 μm high, ~150 μm wide). The rectangular segment where the top channel overlaps with a given pneumatic line constitutes the μFR. When the pneumatic lines are not pressurized (the μFR is "inactive"), the top channels have a normal rectangular cross section [Figs. 1(a)–1(c)]. When the pneumatic lines are pressurized (~30 kPa, compressed air) through computer-actuated miniature solenoid valves (Lee Company, Westbrook, CT),[4] the membrane deflects upwards (the μFR is "activated"), reducing the cross-sectional area of the microchannel to two narrow fluid paths at the top corners [Figs. 1(d)–1(f)]. The μFRs bear similarity with previously reported bistable PDMS microvalves[2–4] that feature either zero or "infinite" resistance; in contrast, the resistance of μFRs can be tuned from zero to a finite value.[5] In principle, a single μFR can be used to tune fluid resistance if the pressurization itself is tuned, but we found it more practical to operate an addressable array of identical μFRs in series combined with a fixed-pressure source.

Our proof-of-concept device features three identical inlet branches (A, B, and C), each containing 15 μFRs in series (~150 μm separation), and one outlet microchannel [Fig. 2(a)]. In our example circuit, all the μFRs are designed with the same dimensions, and they are activated in groups of eight, four, two, or one at a time (such that 16 different resistance values can be encoded with only four pneumatic lines). The number of μFRs activated in branches A, B, and C are termed n_A, n_B, and n_C, respectively. As the ratio $n_A:n_B:n_C$ changes, the relative contributions of each stream to the outlet flow also change [Figs. 2(b)–2(d)], so the position and width of each stream can be modified by the user in real time.[9] In all experiments the inlets are gravity fed by dye reservoirs at equal heights or positively pressurized (amount-

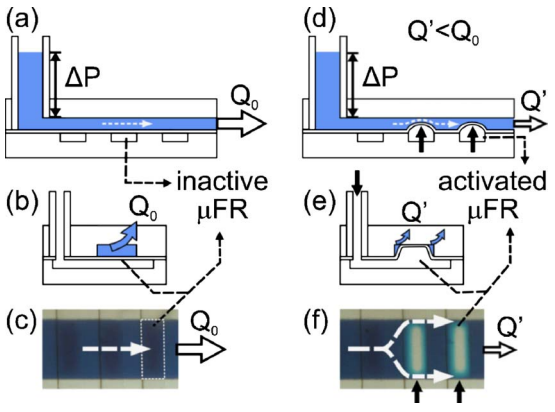

FIG. 1. (Color online) (a) Side-view and (b) front-view conceptual schematics and (c) top-view micrograph of a dye-filled device with inactive (i.e., not pressurized) μFRs; the fluid flow, indicated by a dashed white arrow, is not occluded. (d) Side-view and (e) front-view conceptual schematics and (f) top-view micrograph of a dye-filled device after activating two μFRs (30 kPa, black arrows), showing that the channel is only partially occluded and fluid can flow around the μFRs; the μFRs were manually filled with water prior to being connected to filtered house air through pressure gauges.

[a)]Electronic mail: afolch@u.washington.edu

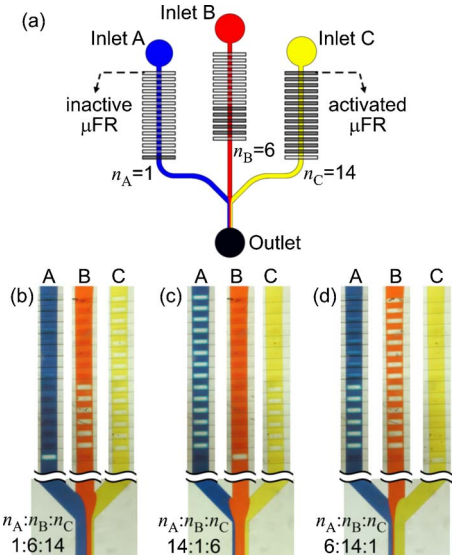

FIG. 2. (Color online) Operation of a μFR device consisting of three inlets that converge into one outlet; before converging, each channel contains 15 μFRs (set at either 0 or 30 kPa), offering 16 resistance settings per branch. The flow is driven at 5 kPa. (a) Schematic top view of the device; the number of μFRs activated in each branch are denoted, from left to right, as n_A, n_B, and n_C. [(b)–(d)] Top-view micrographs of dye-filled channels when n_A:n_B:n_C is (b) 1:6:14, (c) 14:1:6, and (d) 6:14:1.

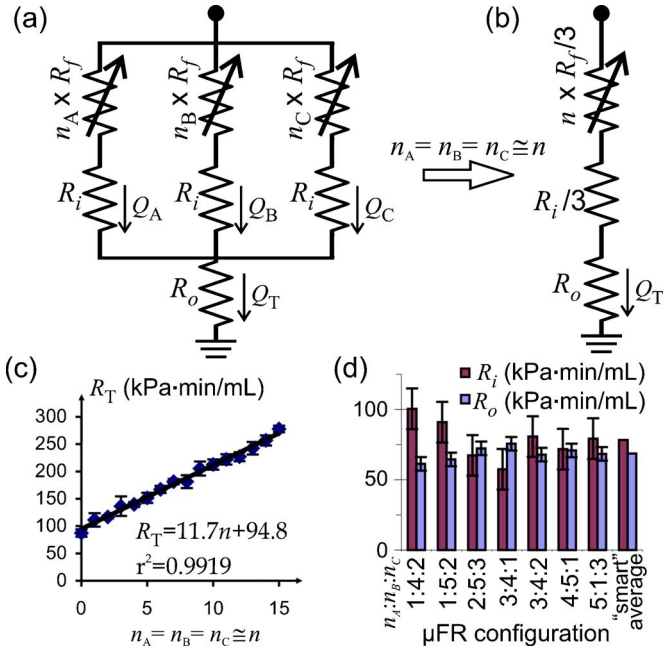

FIG. 3. (Color online) (a) Linear electrical circuit model. Each inlet branch is modeled as a variable resistor (n_xR_f) and a constant resistor (R_i) in series and the outlet channel is modeled as a constant resistor (R_o). (b) When n_A $=n_B=n_C$, the circuit is reduced to three resistors in series. (c) Total flow resistance (R_T) measurements (solid symbols) as a function of the activated number of μFRs n and its linear regression (solid line); the inlets and μFRs are pressurized at 5 and 30 kPa, respectively. (d) R_i and R_o measurements for different μFR configurations n_A:n_B:n_C. The "smart average" is found by averaging the solutions of pairs of equations, one of which is always the linear regression; hence the average also satisfies the linear regression.

ing to a hydrostatic driving pressure ΔP=5 kPa), and the outlet is left at atmosphere, resulting in a flow rate and an average velocity of ~0.052 ml/min and 4.42 cm/s, respectively. We chose this value because it represents the maximum desirable flow velocity for cell culture applications, since it results in shear stresses of 0.45 N/m^2, very close to the lowest values known to compromise surface attachment of adherent cells (0.5–10.0 N/m^2)[10] or to affect cell viability, phenotype, metabolism, and/or protein expression.[11,12] The flow rate has a negligible effect on the μFR resistance values in both the inactive and the activated states. Although at our flow rate the pressure differential driving the flow (5 kPa) causes on the inactive membranes a residual downward deflection of ~19 μm (upstream) or smaller (downstream), fluid dynamics simulations predict that the pressure drop gain caused by each inactive μFR is less than 0.5% (even for infinite flow rates) of the total pressure drop along the whole channel.[9] The active-state upward deflection (which is "saturated" against the microchannel ceiling) is also unaffected by changes in flow rate, probably because in the activated state the membrane portion exposed to fluid (<10% of the whole membrane) is effectively stiffer than the undeflected membrane by orders of magnitude (as expected from the classical elasticity theory[13] and measurements of PDMS membranes[14]). Therefore, for our flow rates or lower, the resistance of the μFRs can be considered independent of the pressure driving the flow and, as a result, independent of position.

For pressure-driven flow in a microchannel, for which the Reynolds number Re is small (Re<1), the steady-state flow rate Q_T is proportional to the driving pressure ΔP.[8] The proportionality constant R_T=$Q_T/\Delta P$ is often referred to as "flow resistance" by analogy with the proportional relationship between voltage difference (ΔV) and electrical current (I) in Ohmic resistances R_Ω=$\Delta V/I$. Assuming infinite microfabrication precision, we model the three-branch device in Fig. 2(a) as an electrical circuit with three inputs at the same ΔV and a common output, one constant resistor R_o (corresponding to the single branch downstream of the μFRs), one constant resistor R_i per inlet branch (corresponding to the inherent resistance of the 2-cm-long branches before activation of μFRs), and a variable resistor per branch equal to the number n of activated μFRs times the resistance R_f of a single μFR [Fig. 3(a)]. Our assumption that all the μFRs have identical resistances is justified experimentally (see below). Kim *et al.* have presented a more sophisticated model of dynamic flow conditions in microfluidic circuits containing elastomeric (compliant) elements represented as capacitances;[15] the absence of capacitors in our model is justified by the fact that we drive the flow at a constant flow rate (thus, the capacitors are "charged"). In our simplified model, the total flow resistance R_T can be expressed as

$$R_T = \frac{1}{1/(n_A R_f + R_i) + 1/(n_B R_f + R_i) + 1/(n_C R_f + R_i)} + R_o. \quad (1)$$

The values R_f, R_i, and R_o must be determined in order to predict the flow rates through branches A (Q_A), B (Q_B), and C (Q_C) and at the output (Q_T) for any given combination of n_A, n_B, and n_C. In principle, R_i and R_o can be determined with analytical formulas[8] if the dimensions of the microchannels are known, and R_f can be computed by fluid dynamics modeling if the deflected membrane's shape is measured. However, measuring these dimensions can be difficult, whereas directly measuring R_T=$Q_T/\Delta P$ in steady state only requires measuring fluid volume at the outlet (10 min average, three to four repeats). In an ideal circuit, three measurements of R_T using any three different combinations of n_A, n_B,

and n_C would suffice to solve for R_f, R_i, and R_o. In practice, only three measurements can yield erroneous Q_T predictions for some n_A, n_B, and n_C values because slight geometrical differences between membranes can result in large membrane deflection differences.[14] Hence, in order to predict R_T values accurately, we find "smart-average" values $\langle R_f \rangle$, $\langle R_i \rangle$, and $\langle R_o \rangle$ and use them instead of R_f, R_i, and R_o when solving the circuit for other values of n_A, n_B, and n_C.

For the special case where the number of activated μFRs in each inlet branch is the same, $n \equiv n_A = n_B = n_C$ [Fig. 3(b)], Eq. (1) is reduced to $R_T[n] = nR_f/3 + R_i/3 + R_o$. A plot of the measured $R_T[n]$ [Fig. 3(c)] for all $n = 0-15$ confirms this linear dependence, $R_T[n] = 11.7n + 94.8$, from which we obtain

$$\langle R_f \rangle = 35.1 \text{ kPa min/ml}$$

and

$$\langle R_i \rangle/3 + \langle R_o \rangle = 94.8 \text{ kPa min/ml}. \quad (2)$$

These averages are smart in the sense that, being based on a linear regression, they give more weight to the points that are closer to the average. Other sets of $n_A \neq n_B \neq n_C$ [there are 4096 combinations; we picked seven sets of low values between 1–5 because low values result in larger changes in R_T, see Eq. (1)] and the corresponding R_T measurements are entered into Eq. (1), forcing the smart $\langle R_f \rangle$ value; for each of these expressions and Eq. (2), we solve R_i and R_o, obtaining (in kPa min/ml) $\langle R_i \rangle = 78.3$ and $\langle R_o \rangle = 68.7$ [Fig. 3(d)]. Note that these values also satisfy Eq. (2).

Despite the simplicity of the model, Eq. (1) and the average R_f, R_i, and R_o values predict the whole range (4096) of flow resistances suprisingly accurately. For example, Q_T can be predicted within 2% for all the permutations of $n_A:n_B:n_C = 1:6:14$,[9] so the three branches are practically indistinguishable. Since Q_A, Q_B, and Q_C can be calculated by Ohm's law once the resistance values are known, the model can also predict mixing and stream "steering" (Fig. 4). The flow rates over a given portion of the channel can be obtained by integration of the flow velocity profile (FEMLAB 3.1, Comsol Inc., Burlington, MA); for instance, if the model predicts that stream A carries 10% of the volumetric flow ($Q_A/Q_T = 0.1$), the left stream will actually span ~12.5% of the channel width.[9] The width and position of stream B, as determined from micrograph measurements [Figs. 4(a) and 4(b)], fall within 4% of the values predicted by the model [Figs. 4(d) and 4(e)]. The same analysis can be extended to the operation of the device as a mixer. If a dye is added to inlet B (branches A and C carrying water) and the dilution of the dye collected at the output is measured using a spectrophotometer, the model-predicted outlet concentration relative to that of inlet B is Q_B/Q_T, which falls within <6% of the measured dilution ratio [Fig. 4(b)]. Importantly, n_A and n_C are virtually interchangeable and the measured Q_B/Q_T is the same for $n_A:n_B:n_C = 0:0:0$ and 6:6:6, indicating that the user can specify the concentration and stream position independently of flow rate.

In summary, μFR arrays allow for controlling flow resistance in microfluidic networks not limited to the simple one demonstrated here. For low flow rates, the steady-state behavior can be accurately predicted using a simple, purely resistive electrical circuit model. Larger arrays of μFRs in series would yield finer levels of flow resistances. We believe that μFRs will be a powerful addition to the microfluidics toolbox for many applications such as cell culture studies, biochemical assays, and biosensors.

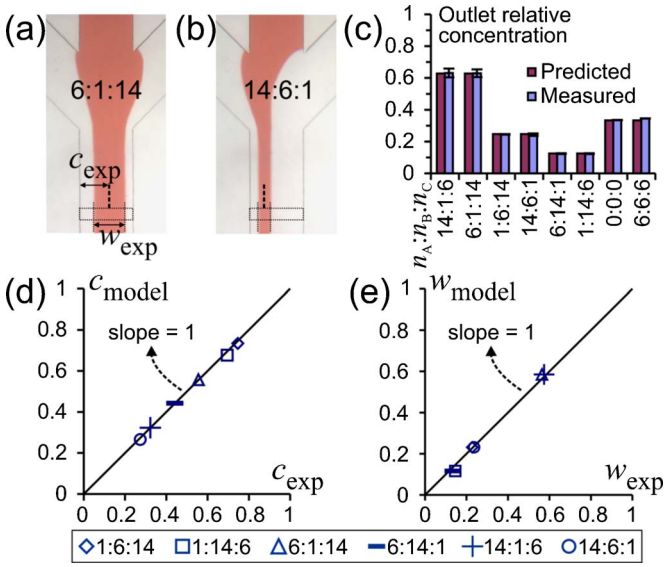

FIG. 4. (Color online) [(a) and (b)] Micrographs showing experimental measurements of stream width w_{exp} and center position c_{exp} for different configurations of $n_A:n_B:n_C$=(a) 6:1:14 and (b) 14:6:1 when the center channel is filled with red dye. (c) Predictions (light bars) and measurements (dark bars) of outlet dye concentration (predicted as Q_B/Q_T) for various $n_A:n_B:n_C$ ratios (0:0:0, 6:6:6, and all the permutations of 1:6:14). (d) Correlation plot of the modeled (c_{model}) vs the experimental (c_{exp}) stream B center position. (e) Correlation plot of the modeled (w_{model}) vs the experimental (w_{exp}) stream B width.

[1] J. C. McDonald, D. C. Duffy, J. R. Anderson, D. T. Chiu, H. Wu, O. J. Schueller, and G. M. Whitesides, Electrophoresis **21**, 27 (2000).
[2] K. Hosokawa and R. Maeda, J. Micromech. Microeng. **10**, 415 (2000).
[3] M. A. Unger, H. P. Chou, T. Thorsen, A. Scherer, and S. R. Quake, Science **288**, 113 (2000).
[4] N. Li, C.-H. Hsu, and A. Folch, Electrophoresis **26**, 3758 (2005).
[5] N. Sundararajan, D. S. Kim, and A. A. Berlin, Lab Chip **5**, 350 (2005).
[6] J. Liu, M. Enzelberger, and S. Quake, Electrophoresis **23**, 1531 (2002).
[7] C.-H. Hsu and A. Folch, Appl. Phys. Lett. **86**, 023508 (2005).
[8] N.-T. Nguyen and S. T. Wereley, *Fundamentals and Applications of Microfluidics* (Artech House, Boston, 2002), p. 471.
[9] See EPAPS Document No. E-APPLAB-89-272642 for material on the measurement of the residual deflection of a valve in the inactive state, the effect of the residual deflection of the inactive μFR on flow resistance, extraction of flow rate ratios from the relative widths of the dye streams, predictions of the total flow rate for various resistance values, and three supplemental movies of the device operating in real time. This document can be reached via a direct link in the online article's HTML reference section or via the EPAPS homepage (http://www.aip.org/pubservs/epaps.html).
[10] J. G. Aunins and H. J. Henzler, *Aeration in Cell Culture Bioreactors*, 2nd ed. (VCH, Weinheim, 1993).
[11] R. M. Nerem, R. W. Alexander, D. C. Chappell, R. M. Medford, S. E. Varner, and W. R. Taylor, Am. J. Med. Sci. **316**, 169 (1998).
[12] J. T. Keane, D. Ryan, and P. P. Gray, Biotechnol. Bioeng. **81**, 211 (2003).
[13] S. P. Timoshenko and J. N. Goodier, *Theory of Elasticity*, 3rd ed. (McGraw-Hill, New York, 1987).
[14] J. M. Hoffman, J. Shao, C.-H. Hsu, and A. Folch, Adv. Mater. (Weinheim, Ger.) **16**, 2201 (2004).
[15] D. Kim, N. C. Chesler, and D. J. Beebe, Lab Chip **6**, 639 (2006).